JOURNAL OF SOLID STATE CHEMISTRY 105, 1–18 (1993)

Electronic Factors Influencing the Local and Cooperative Jahn–Teller Interactions in Spinels with Copper(II) and Nickel(II)*

M. ATANASOV,† U. KESPER,‡ B. L. RAMAKRISHNA,¶ AND D. REINEN‡,§

†*Institute of General and Inorganic Chemistry, Bulgarian Academy of Sciences, Bl.11, Sofia 1040, Bulgaria;* ‡*Fachbereich Chemie und Zentrum für Materialwissenschaften der Phillips-Universität, Hans-Meerweinstr. 1, 3550 Marburg, Germany; and* ¶*Department of Chemistry, Arizona State University, Tempe, Arizona 85287-1604*

Received June 6, 1992; accepted October 27, 1992

Optical spectra and structural data of mixed crystals $Cu_xZn_{1-x}Cr_2O_4$, $Ni_xZn_{1-x}Cr_2O_4$, and $Cu_{1-x}Ni_xCr_2O_4$ are reported. The optical results are used as a probe characterizing the *d*-contributions to the Cu–O bonds. The cooperative Jahn–Teller forces are analyzed, extending the statistical model by Wojtowicz to the tetrahedral sublattice. Thermodynamical and optical data are used to estimate the corresponding cooperative strain energies. A microscopic bonding model is proposed which is based on the bonding properties of the oxygen ligands with respect to Cu^{2+} due to the presence of the "contrapolarizing" Cr^{3+} cations. This concept makes it possible to understand the enhancement of the local Jahn–Teller distortions with increasing cooperativeness.

I. Introduction

The structural phase transitions in spinels MCr_2O_4 ($M = Cu^{2+}$, Ni^{2+}) and mixed crystals $Cu_{1-x}Ni_xCr_2O_4$, with a normal cation distribution (Cu^{2+} and Ni^{2+} occupying exclusively tetrahedral sites), have been studied both structurally (*1–4* and more recently *5*) and by optical spectroscopy (*6, 7*). It is generally accepted that the observed distortions of the MO_4 tetrahedra are due to Jahn–Teller (JT) forces operative in the unit cell. According to the JT theorem, the electronic $^2T_2(a\ ^3T_1)$ ground states of Cu^{2+} (Ni^{2+}) in tetrahedral coordination are geometrically unstable. Their coupling to the normal ε-mode in T_d-symmetry lifts the degeneracy, inducing nondegenerate ground states of lower energy and tetragonally compressed (elongated) geometries for Cu^{2+} (Ni^{2+}).

The cooperative nature of the crystal distortions in these compounds can be rationalized in terms of elastic interactions between the locally distorted polyhedra. Statistical theories of such distortions in spinels (octahedral sites, *8–11*, tetrahedral sites, *12*) and perovskites (*13, 14*) demonstrate that in all cases, where tetragonal structures result from parallel alignments of tetragonally distorted polyhedra in a cubic unit cell (ferrodistortive arrangement), a single long range parameter (σ) describes the structural ordering. Phase transitions are expected to be of first order (latent heat, volume and lattice parameter discontinuities, lambda anomalies of the heat capacity). In cases of E ground states in cubic crystals with antiferrodistortive order patterns second-order cubic-to-tetragonal transitions have been predicted (*11*).

In the so far available theories of the cooperative JT effect it is assumed that each

* A part of this work has been presented at the X[th] International Symposium on the Jahn–Teller Effect, Kishinev, September, 1989.

§ To whom correspondence should be addressed.

0022-4596/93 $5.00

polyhedron possesses its own local distortion, ground state splitting, and stabilization energies, which persist in the low-symmetry phase. The structural phase transitions appear as a consequence of coupling of local electronic states to bulk deformations and optical phonons of the lattice. The results from optical spectra of many systems (*6, 7, 15, 16*) demonstrate, however, that large shifts of the ligand field transitions to higher or lower energies are observed with increasing concentration of the JT ion in host structures with interconnected polyhedra. Cooperative alignment of distorted polyhedra leads to phases of lower symmetry below the transition temperature (T_C) with considerably enhanced or reduced local JT distortions.

In spite of the models available, the physical origin of the large local and crystal distortions in MCr_2O_4 ($M = Cu^{2+}$ and Ni^{2+}) is far from being well understood. Especially, the large structural distortions for $CuCr_2O_4$ and the high T_C of ≈900 K are rather surprising in view of the weak direct interactions of the CuO_4 tetrahedra, separated from each other by (non-JT) Cr^{3+} ions. The present work tries to contribute to the understanding of this phenomenon by looking at the local M–O ($M = Cu^{2+}$, Ni^{2+}, Cr^{3+}) bonding changes accompanying the phase transition. In particular, the influence of the bonding properties of the interconnecting oxygen ligands on the extent of the local distortion and their enhancement by the cooperative strain is analyzed. Thermodynamic and optical data are used to calculate the cooperative strain energies. The cooperative JT forces are characterized, extending the statistical model by Wojtowicz (*9*) to the tetrahedral sublattice. The experimental basis is the spectroscopic data as well as phase diagrams for the mixed crystal series $Zn_{1-x}M_xCr_2O_4$ ($M = Cu^{2+}$, Ni^{2+}) and $Ni_{1-x}Cu_xCr_2O_4$ as a function of T and x, which we report in the following. The optical spectra are used as a probe characterizing the M–O bonds in the surrounding of the next nearest cations ($M(OCr_3)_4$ moieties) as well.

In a second paper the influence of cooperative JT distortions on the bulk magnetic properties, such as ordering temperatures, will be discussed on the basis of susceptibility data.

II. Experimental Section

Preparation. Mixed crystals $Zn_{1-x}M_xCr_2O_4$ ($M = Cu^{2+}$, Ni^{2+}) and $Cu_{1-x}Ni_xCr_2O_4$ were synthesized by the slow evaporation of mixtures of nitrate solutions with Ni^{2+}, Cu^{2+}, Zn^{2+}, and Cr^{3+} in the respective molar ratios, decomposition of the solid nitrates, and subsequent heating of the reactive and thoroughly intermixed oxides. The mixtures were heated for 15–20 hr at 950–1000°C in flowing oxygen, finely mortared, and sintered again under the same conditions, but in air. The compounds with Cu^{2+} concentrations $x \geq 0.9$ were heated at 900°C, because they partly decomposed (formation of Cu^{1+}) otherwise.

Structural characterization. The mixed crystals were characterized by X-ray diffractometry and Guinier technique (calibration by Si and BaF_2, respectively) and were single-phase. The Guinier technique was applied between 1300 and 150 K.

Optical spectroscopy. Powder reflectance spectra were recorded between 4000 and 25,000 cm^{-1} and at 298 and 5 K by a Zeiss PMQ II spectrophotometer (with a low-temperature accessory). The reflectance data are transformed into log k/s-values according to the theory of Kubelka and Munk (k and s: absorption and scattering coefficient, respectively).

III. Results

1. Mixed Crystals $Zn_{1-x}Cu_xCr_2O_4$

Structural data and ligand field spectra have been reported for this mixed crystal series already (*6, 7*). Figure 1 shows the phase diagram. The cubic to tetragonal phase transitions are discontinuous above $x \approx 0.3$ and there is always a temperature

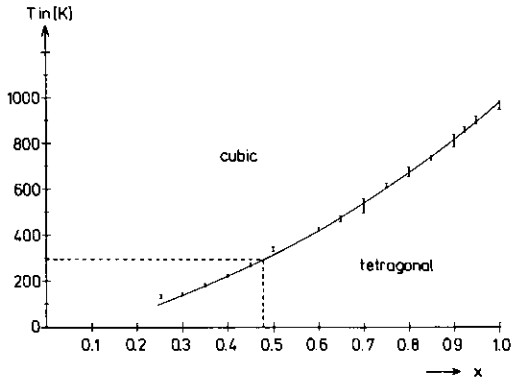

FIG. 1. Phase line of the tetragonal ($c/a < 1$) to cubic transition for mixed crystals $Zn_{1-x}Cu_xCr_2O_4$.

region where the two phases coexist—which is probably caused by the finite heating or cooling rates. The phase change of $CuCr_2O_4$ occurs at 965 ± 20 K, somewhat higher than the value reported in the literature (T_c = 920 K (*3*)). Some selected ligand field spectra are depicted in Fig. 2. The *d–d* transitions due to tetrahedral Cu^{2+} are nicely resolved below the charge-transfer region, which extends down to about 11,000 cm^{-1}—overlapping the octahedral Cr^{3+} absorption—and which is responsible for the dark color of the mixed crystals. The two bands, observed at 4900 and 8600 cm^{-1} for $x = 1.0$, shift to lower energies with decreasing Cu^{2+}content as the consequence of a diminishing influence of cooperative Jahn–Teller forces (see below). The two bands have to be assigned to the two symmetry-allowed *d–d* transitions $^2B_2 \rightarrow {}^2E$ and $^2A_1$, respectively, in a compressed D_{2d} site (*6–7*). $^2B_2$ and ^2E are the split state of the tetrahedral $^2T_2$ ($e^4t_2^5$) ground state, while $^2A_1$ and $^2B_1$ arise from the excited ^2E (e^3t^6) state. The dependence of the band positions on x (298 K) is depicted in Fig. 3. The first order nature of the phase transitions becomes apparent also in the abrupt change of the $^2B_2 \rightarrow {}^2A_1$ band position at the critical concentration of the phase transition (298 K) x = 0.48 (Figs. 1, 2). In this region the transition becomes asymmetric, indicating a distribution of Cu^{2+} clusters within the mixed crystal. This is nicely demonstrated by comparing the 298 and 5 K reflectance spectra for x = 0.45, for example. While the peak at 6400 cm^{-1} is characteristic for a "local" CuO_4 polyhedron that is not embedded in cooperative Jahn–Teller interactions with neighboring copper polyhedra, the shoulder around 7200 cm^{-1} is due to clusters with a ferrodistortive order, which are still present in the cubic phase. The low-temperature spectrum shows just one band at the position of the shoulder–in accordance with the existence of long-range cooperative ordering induced by the cooling below the transition temperature. At concentrations $x > 0.5$ only small higher-energy shifts of the band positions are observed going from 293 to 5 K. The noticeable width of the $^2B_2 \rightarrow {}^2A_1$ band for x = 0.9 at 295 K is presumably again caused by a cluster distribution.

The ligand field spectra below 11,000 cm^{-1} show no indication that absorptions other than those of tetrahedral Cu^{2+} are present. We cannot confirm the finding of Lenglet *et al.* (*17*) that a small exchange of Cr^{3+} and Cu^{2+} between octahedra and tetrahedra occurs. The presence of octahedral Cu^{2+} would clearly show up in addition to the tetrahedral bands, as has been discussed in (*5*) already and as has been demonstrated for various Cu^{2+} doped spinel and garnet host compounds (*18*). It should be emphasized, however, that a careful preparation of the mixed crystals is necessary (see Section II) in order to obtain reproducible results.

A formal treatment of the interplay between the local and cooperative Jahn–Teller effects in this mixed crystal series is given in Section IV.

2. *Mixed Crystals* $Zn_{1-x}Ni_xCr_2O_4$

Structural and ligand field data have been reported already (*5, 7*) and are discussed elsewhere with respect to the local and cooperative Jahn–Teller effects (*7*). It has been shown that the local effect is suppressed by configurational mixing with the excited $^3T_1$ state and LS coupling, and that

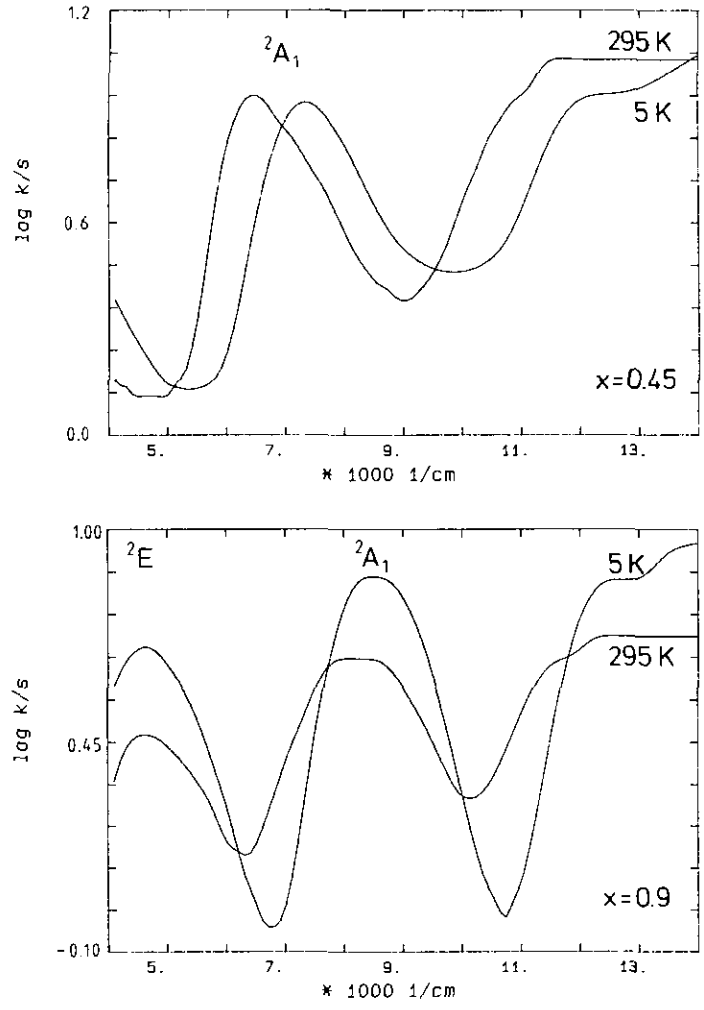

FIG. 2. Ligand field reflectance spectra of mixed crystals $Zn_{1-x}Cu_xCr_2O_4$.

only the influence of cooperative interactions leads to small ground state splittings and distortions. Figure 4 shows the phase line for the mixed crystal series. The critical temperature of $NiCr_2O_4$ for the tetragonal to cubic phase transition is $T_C \approx 335$ K and decreases rapidly with decreasing Ni^{2+} concentration. The transition is discontinuous. The ligand field transitions do not shift significantly with x as expected for the weak cooperative forces (*7*).

3. *Mixed Crystals* $Cu_{1-x}Ni_xCr_2O_4$

The structural behavior of this series is very interesting, because Jahn–Teller forces stabilize tetragonally compressed and elongated tetrahedra in the cases of Cu^{2+} and Ni^{2+}, respectively. The interplay between these two diverging tendencies leads from a tetragonal structure with $c/a < 1$ to a tetragonal lattice with $c/a > 1$ via an orthorhombic region with decreasing Cu^{2+} concentration (*19, 5*). The corresponding phase diagram, redetermined by us, is depicted in Fig. 5. Compared to the one in (*12*) the phase line for the tetragonal to cubic phase is shifted to higher temperatures (vide supra).

The existence of an orthorhombic phase is explained as follows. Figures 6a and 6b

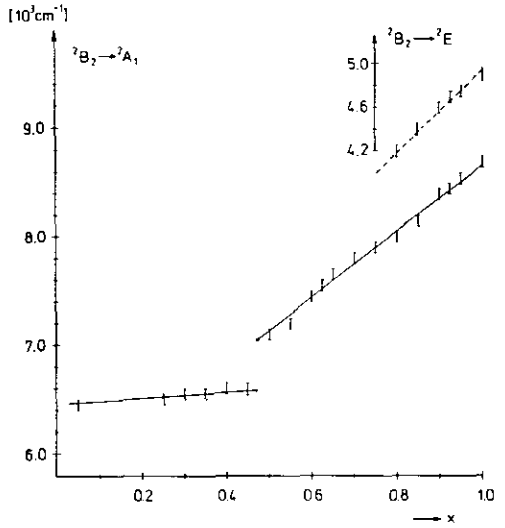

FIG. 3. Dependence of the d–d transition energies of Cu^{2+} on x for mixed crystals $Zn_{1-x}Cu_xCr_2O_4$.

(dashed lines) depict features of the ground state potential surface of a polyhedron with a T ground state, which is vibronically coupled with a vibrational ε mode in T_d symmetry (*19*). The potential surface can be modified by strains, as imposed on the system by a unit cell distortion, for example. The ferrodistortive order of tetragonally compressed CuO_4 tetrahedra in $CuCr_2O_4$ (minimum at 180°—Fig. 6a, full curve) is disturbed by the incorporation of Ni^{2+} with increasing x, which imposes a cooperative strain with the symmetry of $\varphi = 120°$ (or 240°) at higher Ni^{2+} concentrations. This leads to a shift of the Cu^{2+} minimum at 180° toward 120°, implying an orthorhombic distortion component (Figs. 6e, 6g). Starting from $NiCr_2O_4$ ($x = 1.0$, ferrodistortive order of elongated tetrahedra, minimum at 120°—Fig. 6b, full curve) and looking at Ni^{2+}, the strain imposed on the NiO_4 tetrahedra at $\varphi = 180°$ (or 60°) by the substituting Cu^{2+} ions shifts the minimum at 120° toward 180° (Figs. 6f, 6h), again inducing an orthorhombic symmetry. The location of the orthorhombic phase region at rather high x-values reflects the much stronger Jahn–Teller effect of Cu^{2+} compared to Ni^{2+}. A more detailed analysis of the potential surfaces of CuO_4 and NiO_4 polyhedra in the presence of cooperative strains and their significance for the phase diagram (Fig. 5) is given in Section IV.4.

We can translate the given complex description into a very simple picture. If Ni^{2+} ions are substituted into $CuCr_2O_4$, they will tend to distort their sites, which are tetragonally compressed by the Cu^{2+} influence, toward an elongation. The easiest way to accomplish this is to choose one of the two C_2 axes perpendicular to the S_4 axis of compression, because these are directions of elongation already. This will necessarily lead to a D_2 symmetry.

The phase transitions are discontinuous up to intermediate and at very high x-values. They are of second order in the concentration range of the orthorhombic structure ($0.70 < x < 0.90$), and changes of the unit cell parameters occur over a wide temperature range (Fig. 7).

It is immediately apparent from the comparison of the phase diagrams in Figs. 1 and 5 that the substitution of Zn^{2+} by Ni^{2+} considerably enhances the critical temperatures for the transition to the cubic spinel structure. In contrast to Zn^{2+}, Ni^{2+} does not destroy the cooperative forces and supports a considerable local Jahn–Teller distortion of

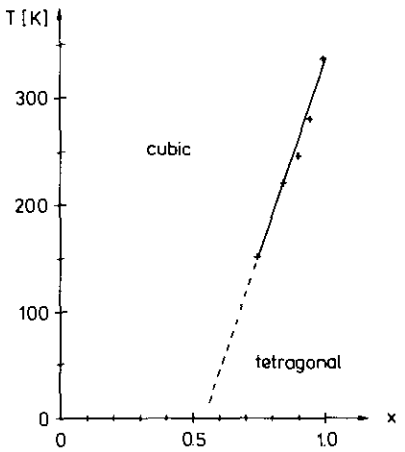

FIG. 4. Phase line of the tetragonal ($c/a > 1$) to cubic transition for mixed crystals $Zn_{1-x}Ni_xCr_2O_4$.

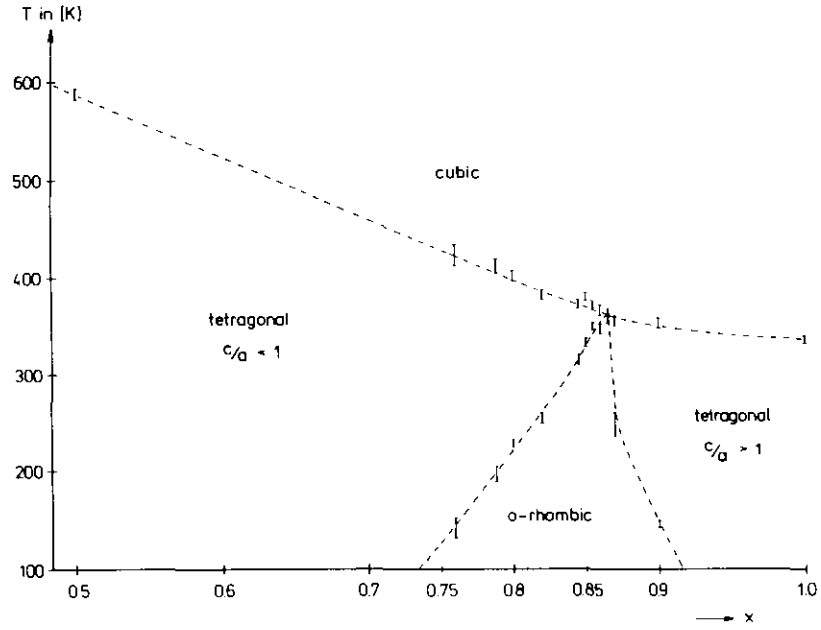

FIG. 5. Phase diagram of mixed crystals $Cu_{1-x}Ni_xCr_2O_4$.

the CuO_4 tetrahedra. This is also nicely reflected by the ligand field spectra, where the *d–d* bands of Cu^{2+} and Ni^{2+} are observed side by side (Fig. 8). In particular the transitions ${}^2B_2 \rightarrow {}^2A_1$ (I) and ${}^3{}_gA_2 \rightarrow {}^3B_1$ (II) of Cu^{2+} and Ni^{2+} (D_{2d} assignment: compression and elongation), respectively, are well resolved. Transition II for Ni^{2+} always appears between 8200 and 9000 cm^{-1} (dependent on x and T) because of a vanishing local and only a small cooperative Jahn–Teller contribution.

The energy of the Cu^{2+} band I varies widely (295 K) from 6600 cm^{-1} ($x = 0.95$) to 8600 cm^{-1} ($x = 0$). The band energies are higher than those of mixed crystals $Zn_{1-x}Cu_xCr_2O_4$ with the same Cu^{2+} concentrations (compare Fig. 3), which implies that the local distortions of the CuO_4 polyhedra are indeed larger than those in the Zn^{2+} compounds. As expected, Ni^{2+} "supports" a stronger Jahn–Teller distortion of the CuO_4 tetrahedra by the cooperative forces imposed on the spinel lattice.

Band II and in particular band I shift to considerably higher energies with decreasing temperature (Fig. 8). The presumable reason is the "freezing-in" of dynamic distortion components into local orthorhombic polyhedra deformations at low temperatures, which become cooperative in the region $x \approx 0.82 \pm 0.12$ at 5 K (extrapolation from Fig. 5). The band shift to higher energies is due to the additional cooperative Jahn–Teller contributions, which are induced by the orthorhombic unit cell distortions and which increase with decreasing temperature (Fig. 7). Unfortunately the transition between the split states of the tetrahedral ${}^2T_2$ parent ground term lies below 4000 cm^{-1} and is not detectable in the accessible spectral region above $x \approx 0.2$.

IV. The Origin of the Cooperative Jahn–Teller Effect in Spinel Mixed Crystals $M_xZn_{1-x}Cr_2O_4$ ($M = Cu^{2+}$, Ni^{2+})

1. The Statistical Model of Woitowitz for Tetrahedral Sites

In a normal spinel AB_2O_4 (A^{2+} (B^{3+}) ions occupying T_d (D_{3d}) sites) the A^{2+} lattice can be subdivided into two interpenetrating nonequivalent face-centered cubic lattices 1 and 2. A cation of any one of these sublattices

is tetrahedrally surrounded by four cations from the other one. In the presence of a static distortion of each tetrahedron in the cubic lattice, with a statistical distribution of the S_4 axes along the unit cell directions, two interaction potentials between neighboring JT centers V_{11} and V_{12} can be defined, refering to mutually parallel and perpendicular orientations of the S_4 axes, respectively. Since the JT ions are interconnected by O–*B*–O bridges, there will be distinct elastic and electronic contributions to V_{11} and V_{12} from the non-JT ions, modifying the Cu–O bonds and influencing the effective coupling between neighboring JT centers in dependence on the Cu^{2+} (Ni^{2+}) concentration.

The configurational energy (T = O K) is given by

$$H = pV_{11} + qV_{12} \tag{1}$$

where p and q are the total number of nearest neighbor contacts contributing to V_{11} and V_{12}, respectively. For a distribution of S_4 axes given by the occupation variables $\mathbf{N} = N_1^\nu, N_2^\nu$ ($\nu = x, y, z$) the probability of an S_4^x orientation of a site of sublattice 2 is $N_2^x/(N/2)$. The number of pairs with the S_4 axes parallel to x is then $ZN_1^xN_2^x/(N/2)$ (Z: coordination number of each site with respect to the others ($Z = 4$)). It follows that

$$p = (8/N)\sum_\nu (N_1^\nu N_2^\nu), \tag{2}$$

$$q = (8/N)\sum_{\nu>\nu'} (N_1^\nu N_2^{\nu'} + N_1^{\nu'} N_2^\nu).$$

The determination of the equilibrium values of $\mathbf{N}$ is considerably simplified by the fact that all configurations can be expressed in terms of a single long-range parameter (for $N_i^x = N_i^y$ with $i = 1, 2$):

$$\sigma = (N_i^z - N_i^x)/(N/2), \quad i = 1, 2. \tag{3}$$

Since $\sum_\nu N_i^\nu = N/2$ one obtains

$$N_1^x = N_1^y = N(1 - \sigma)/6$$
$$N_i^z = N(1 + 2\sigma)/6. \tag{4}$$

The substitution into Eqs. (2) and (1) yields

$$p = (\tfrac{2}{3})N(1 + 2\sigma^2), \quad q = (\tfrac{4}{3})N(1 - \sigma^2) \tag{5}$$

$$H = (\tfrac{2}{3})N(V_{11} + 2V_{12}) + (\tfrac{4}{3})\sigma^2(V_{11} - V_{12}). \tag{6}$$

Introducing thermal populations of excited state configurations and applying a theory described elsewhere (*19*) results in the expression for the free energy

$$\frac{F(\sigma) - F(0)}{2kTN/3} = (1 - \sigma)\ln(1 - \sigma) + (\tfrac{1}{2})(1 + 2\sigma)\ln(1 + 2\sigma) - \frac{\sigma^2}{2J} \tag{7}$$

with the free energy of the cubic phase

$$F(0) = -kT\ln 3 + (2N/3)(V_{11} + 2V_{12}) \tag{8}$$

and the reduced temperature

$$J = (\tfrac{1}{4}\ln 2)\cdot\frac{T}{T_c} = \frac{kT}{4(V_{12} - V_{11})}. \tag{9}$$

It can be seen by comparison with earlier results (JT ions in octahedral sites (*9*)) that $F(\sigma)$ and J are smaller by a factor of 2. The equilibrium values of σ at any temperature are obtained by minimizing $F(\sigma)$ with respect to σ at constant J,

$$\frac{1 + 2\sigma}{1 - \sigma} = \exp\left(\frac{\sigma}{J}\right), \quad 0 \leq \sigma < 1 \tag{10}$$

which is the same result as for the octahedral case, but with the mentioned difference in the reduced temperature. The critical temperature for the phase transition is derived by setting $F(\sigma) = F(0)$ in Eq. (7) and making use of Eq. (10). The conditions reflect the usual requirement for the coexistence of two phases (cubic and tetragonal) at a finite σ, yielding $\sigma = (\tfrac{1}{2})$ at the phase transition and, after substitution into Eq. (9), also the reduced temperature at the phase transition

$$J_c = \mathrm{I}/(4\ln 2) = 0.3607. \tag{11}$$

Above J_c only the cubic phase is stable, while below J_c the tetragonal phase ($\sigma > \frac{1}{2}$) is observed. The temperature dependence of the lattice parameters can be obtained if

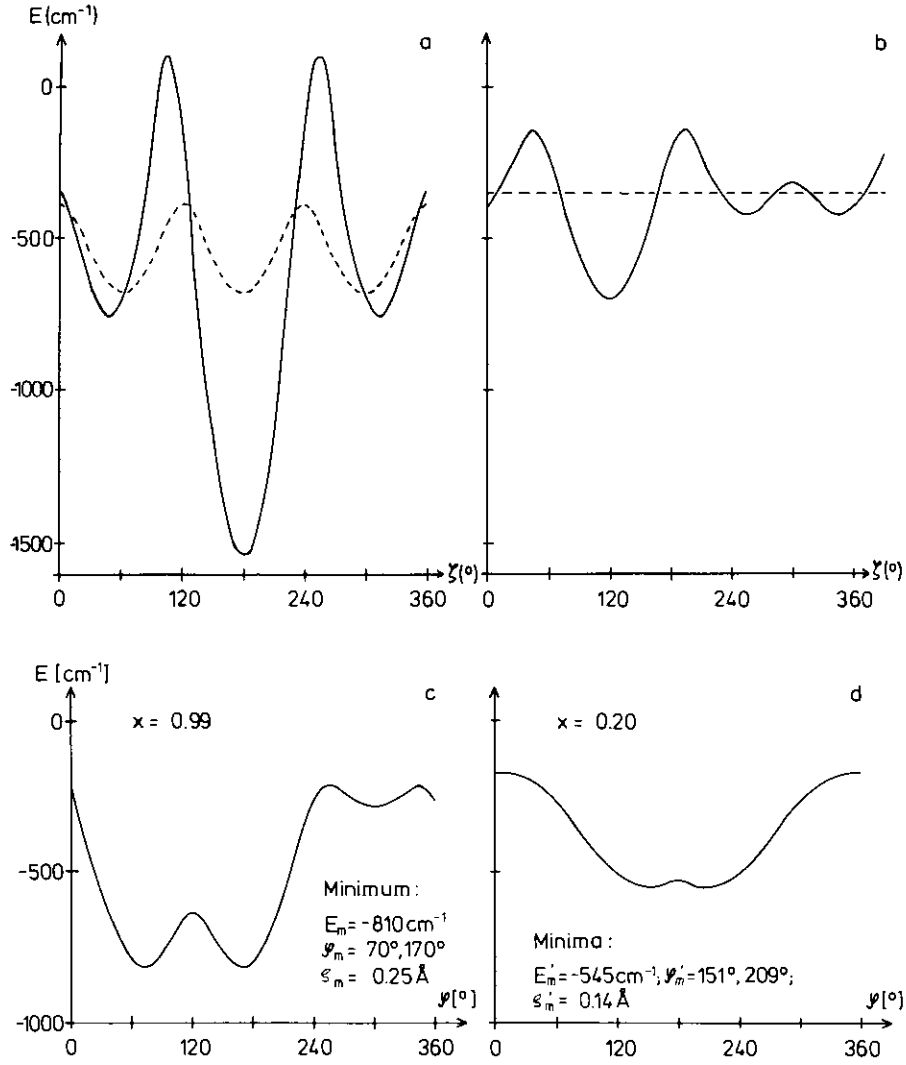

FIG. 6. The ground state potential surfaces of the CuO_4 and NiO_4 tetrahedra in mixed crystals $Cu_{1-x}Ni_xCr_2O_4$ (the angular dependence of the ground state energies at ρ_m (ρ'_m)). The chosen parameters are K_e = 16,450 cm^{-1} Å^{-2}; $V_e^{Cu\,(Ni)}$ = −4300 (2900) cm^{-1} Å^{-1}; ζCu (Ni) = −650 (−450) cm^{-1} (7). The following concentration-dependent strain coefficients, originating from cooperative Jahn–Teller interactions, were used (see Eq. (28) for definitions): $S_{Cu\,(Ni)}$ = −2700 (1700) cm^{-1} Å^{-1}. (a) Local Jahn–Teller distortion of CuO_4 tetrahedra without (ρ_m = 0.26 Å, dashed curve) and with (ρ_m = 0.42 Å, solid curve) cooperative strain. (b) Local distortion of the NiO_4 tetrahedra without (ρ'_m = 0, dashed line) and with strain (ρ'_m = 0.26 Å, solid line). (c (d)) Local distortion of the CuO_4 (NiO_4) tetrahedra at x = 0.99 (0.20); the symmetrical orthorhombic minima indicate tetragonal geometries in the dynamical average. (e–h) Distortions of the CuO_4 (left) and NiO_4 polyhedra (right) at x = 0.70 and x = 0.85.

proportionality between the average tetragonal unit cell parameters a, c and the mean lengths of the tetrahedral distortion axes parallel and perpendicular to S_4 is assumed,

$$\frac{c}{a} = \frac{3 + (\gamma - 1)(1 + 2\sigma)}{3 + (\gamma - 1)(1 - \sigma)} \approx 1 + (\gamma - 1)\sigma \quad (12)$$

where γ is the c/a ratio at T = 0 K.

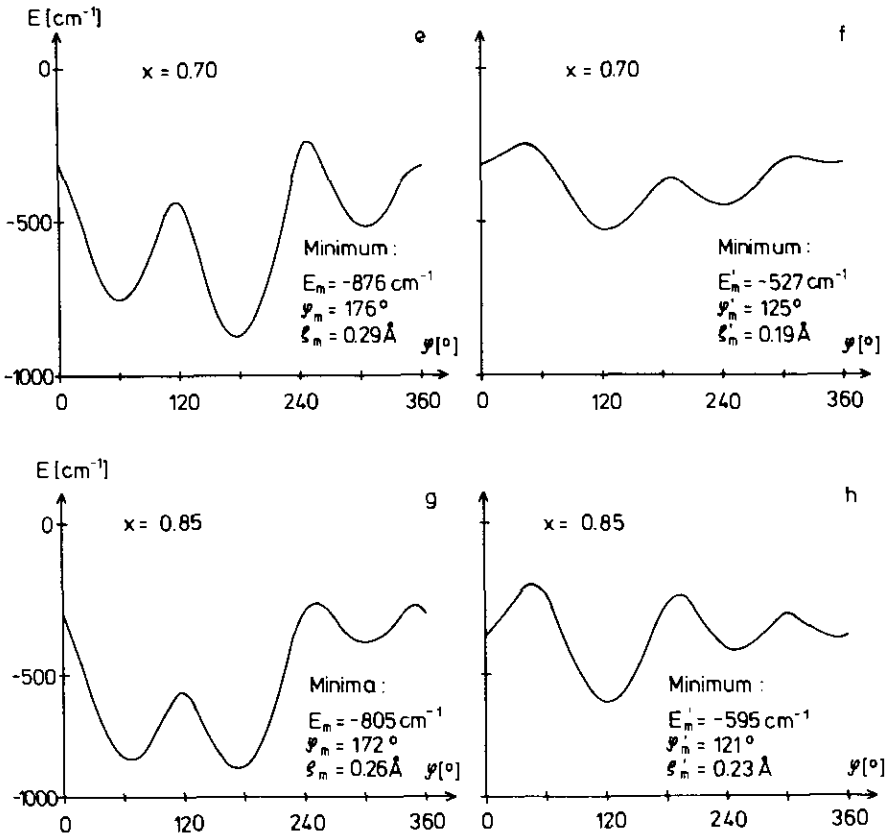

FIG. 6—*Continued*

Equations (9)–(12) are used in connection with the optical spectra to get information about the bonding in the JT polyhedra and how it is influenced by the cooperativity.

For mixed crystals $M_xZn_{1-x}Cr_2O_4$ the thermodynamic equations (7), (9), (11), and (12) retain their validity, but the ordering parameter σ and the transition temperature

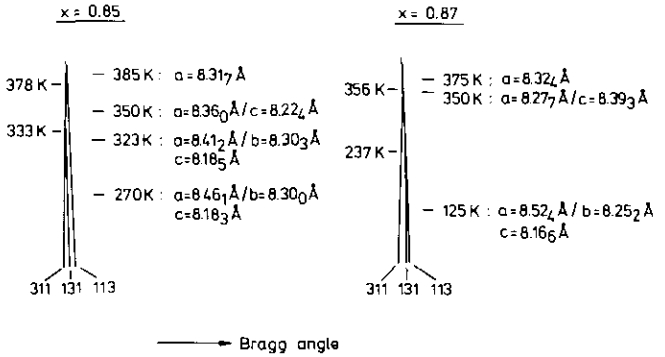

FIG. 7. The cubic to tetragonal to orthorhombic phase changes (Guinier diagrams; (311) reflections) for mixed crystals $Cu_{1-x}Ni_xCr_2O_4$ (x = 0.85 left, 0.87 right).

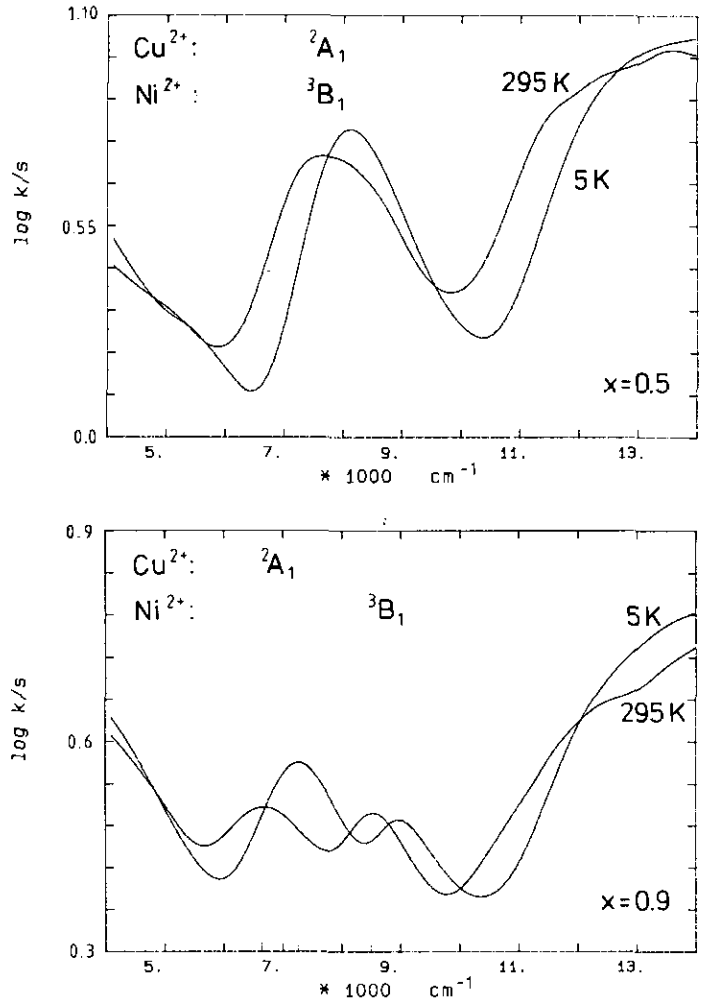

FIG. 8. Ligand field reflectance spectra of mixed crystals $Cu_{1-x}Ni_xCr_2O_4$ ($x = 0.5; 0.9$). The transitions a^3A_2 (a^3T_1) $\rightarrow$ $^3B_1$ ($^3A_2$) and $^2B_2$ ($^2T_2$) $\rightarrow$ $^2A_1$ (^2E) for Ni^{2+} and Cu^{2+}, respectively, are marked.

J_c are claimed to be multiplied by x (see next sections, however).

2. *Cooperative Strain Energies in Mixed Crystals $Zn_{1-x}M_xCr_2O_4$*

In this section we describe an approach that makes it possible to determine cooperative strain energies (S) and geometric distortions (ρ), making a combined use of spectroscopic and thermodynamic data. Let us consider mixed crystals $Zn_{1-x}M_xCr_2O_4$ (M: Cu^{2+}, Ni^{2+}). The oxygen ligands in the spinel structure are involved in four pseudotetrahedral σ-bonds (to one Cu^{2+} and three Cr^{3+}). Hence π-bonding contributions to the Cu–O bond may be neglected in first order. The following transition energies result,

$$\Delta E(^2B_2 \rightarrow {}^2E) = (\tfrac{3}{2})\,|V_e^{\text{eff}}\rho|$$

$$\Delta E(^2B_2 \rightarrow {}^2A_1) = |V_e^{\text{eff}}\rho| + \Delta_t, \qquad (13)$$

where ρ is the radial JT distortion parameter,

$$\rho = |Q_\theta| = R\,|2\theta_t - 2\theta|, \qquad (14)$$

2θ is the angle bisected by the S_4 axis

$[2\theta_t = 109.47°]$, $|V_e^{eff}|$ the (effective) linear vibronic constant (*7*), and Δ_t the cubic ligand field splitting. Using Eq. (13) and the observed transition energies ($M = Cu^{2+}$, Fig. 3) we obtain Δ_t and $|V_e^{eff}\rho|$ as a function of x ($x > 0.45$; in cm^{-1}):

$$|V_e^{eff}\rho| = 750 + 2500\,x,$$
$$|\Delta_t| = 4750 + 650\,x. \qquad (15)$$

While Δ_t shows minor variations with x, reflecting the slightly larger ionic radius of Zn^{2+} compared to Cu^{2+} and hence the corresponding matrix effect, the tetragonal ligand field $|V_e^{eff}\rho|$ increases significantly due to cooperative forces. The influence of the ferrodistortive ordering of compressed (elongated) tetrahedra with S_4 axes along the z (x) direction on the energy levels of Cu^{2+} (Ni^{2+}) can be accounted for formally by a diagonal matrix H_s (*7, 20*),

$$T_2\xi[T_1\alpha]: (\tfrac{1}{2})S_c\rho\cos\varphi_s\,[-S_c'\rho\cos(\varphi_s' - 120°)]$$
$$T_2\eta[T_1\beta]: (\tfrac{1}{2})S_c\rho\cos\varphi_s\,[\tfrac{1}{2}S_c'\rho\cos(\varphi_s' - 120°)] \qquad (16)$$
$$T_2\zeta[T_1\gamma]: -S_c\rho\cos\varphi_s\,[(\tfrac{1}{2})S_c'\rho\cos(\varphi_s' - 120°)],$$

with the definitions $S_c < 0$ ($S_c' > 0$) and fixing the absolute minima at the positions $\varphi_s = 180°$ ($\varphi_s' = 120°$). The strain energies $S_c\rho$ ($S_c'\rho$) reflect the cooperative interactions of a given JT center with other distorted centers of the same kind. It is to be emphasized that these energies are proportional to the radial distortion parameter. This implies that the local Jahn–Teller distortion may depend on the strength of the cooperative interactions—as is indeed experimentally found. Making use of the models by Wojtowicz for tetrahedral sites (Section IV.1) and of Kanamori (*12*), one can connect the strain energy $|S_c|\rho$ (Eq. (16)) with the pair energy $V_{12} - V_{11}$ and the critical temperature T_c,

$$(V_{12} - V_{11})/kT_c = \ln 2 \qquad (17a)$$
$$|S_c(x)|\rho(x) = 8\,(V_{12} - V_{11})/3 \qquad (17b)$$
$$kT_c = (3/8\ln 2)|S_c(x)|\rho(x) \qquad (17c)$$

where x denotes the Cu^{2+} or Ni^{2+} concentration in the Zn^{2+} matrix (substitution of S_c by S_c' for Ni^{2+}). From the phase transition temperature, T_c ($x = 1$) = 965 K (Fig. 1), one gets $|S_c|\rho = 1200\ cm^{-1}$. Considering V_e^{eff} as a sum of local V_e and cooperative contributions S_c, $|V_e^{eff}| = |V_e| + |S_c|$, one calculates $V_e = -4700\ cm^{-1}\,Å^{-1}$ and $S_c = -2700\ cm^{-1}\,Å^{-1}$ from the radial distortion parameter $\rho = 0.44$ Å and by using Eq. (13). Since higher order vibronic coupling is comparatively small and the local force constant, by definition (see below), does not vary with x, we may estimate the radial JT distortion parameter ρ as a function of the concentration x,

$$\rho(x) = (|V^{eff}|\rho(x) - |S_c|\rho(x))/|V_e|, \qquad (18)$$

where $|V^{eff}|\rho(x)$ is taken from the optical spectrum (Eq. (13)) and $|S_c(x)|\rho(x)$ is calculated from the critical temperatures (Eq. (17c)). Figure 9 illustrates the x-dependence of ρ and S_c. $\rho(x)$ increases with x, indicating that the local Jahn–Teller distortion is significantly enhanced by the cooperativity, but in a nonlinear fashion. $S_c(x)$ seem to be linearly dependent on x in first approximation. The extrapolation indicates that $S_c(x)$ becomes zero at $x \approx 0.1$ (at O K). Recall that the effective force constant of the Jahn–Teller active ε mode is

$$K_e = |V_{eff}(x)|/\rho(x). \qquad (19)$$

K_e is also accessible in dependence on x. It is found to be constant within the error limits ($16{,}700 \pm 850\ cm^{-1}\,Å^{-2}$). The derived vibronic parameters V_e, S_c, and K_e are very similar to those calculated by a different approach and on the basis of slightly differing experimental data (*7*).

Combining Eqs. (9) and (10), the ordering parameters result as a function of x, with $T_c(x)$ and $J(x)$ taken from the experiment. Then Eq. (12) makes it possible to calculate the c/a ratios as functions of x, which are in good agreement with the experimental

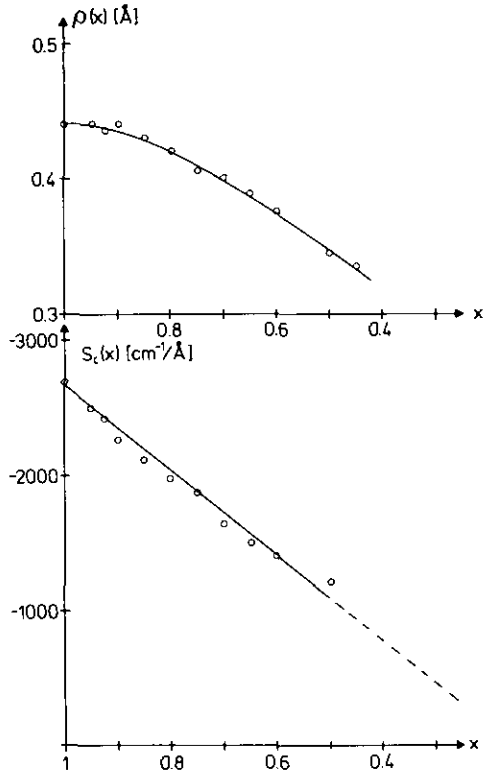

FIG. 9. The dependence of ρ and S_c on the Cu^{2+} concentration in mixed crystals $Zn_{1-x}Cu_xCr_2O_4$.

values (6). If the c/a values are calculated assuming $T_c(x) = x \cdot T_c$ (Section IV, 1), the extrapolated c/a ratio for $x = 1$ is much larger than the experimental one, reflecting again the increase of the local ρ parameter with increasing Cu^{2+} concentration.

The radial distortion parameter is about $\rho = 0.33_5$ Å at the phase transition ($x = 0.47$, 298 K) in the cooperative region and drops to $\rho \approx 0.28$ Å passing T_c.

Analogous considerations are valid for $Zn_{1-x}Ni_xCr_2O_4$ mixed crystals, though the effects are considerably less pronounced due to the smaller $V_e'(x)$ and $S_c'(x)$ values (7).

3. The Origin of the Enhancement of the Local Jahn–Teller Distortion by Cooperative Interactions—A Microscopic Bonding Model

The enhancement of the ground state splitting and of the local Jahn–Teller distortion with increasing x in mixed crystals $Zn_{1-x}M_xCr_2O_4$ (M: Cu^{2+}, Ni^{2+}) can be understood by the following microscopic bonding model. Figure 10 illustrates the pseudotetrahedral cationic coordination of the spinel oxygen atoms and how the elastic and electronic interactions between the tetrahedra are mediated by interconnecting

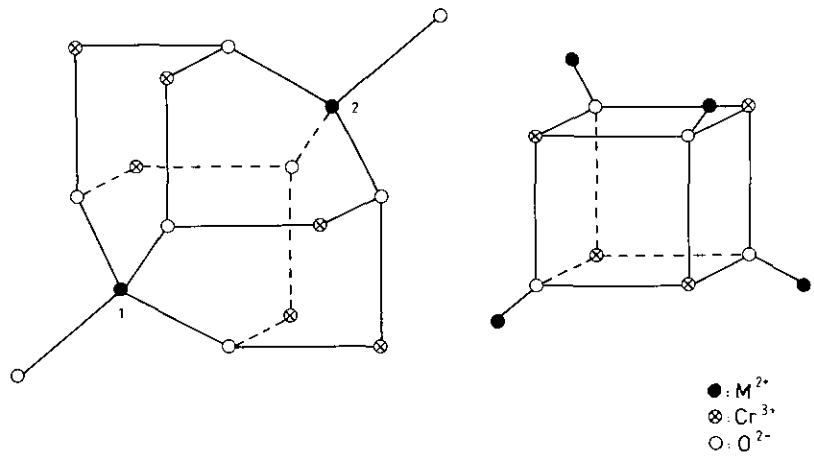

FIG. 10. Sections from the spinel structure: the bridging geometry between two tetrahedral M^{2+} ions ($(OMO_3Cr_6O_3MO)$ cluster, left) and the coordination geometry of oxygen with respect to M^{2+} and Cr^{3+} in the cubic structure with an ideal oxygen positional parameter (right).

TABLE I

BOND ANGLES (°) AND DISTANCES (Å) IN SPINELS MCr_2O_4

M	2θ	$R(M\text{–}O)$	a_y	a_x	a_z	α_{xy}	α_{yz}	α_{xz}
Cu	122.4	1.94	2.055	1.995	1.99	97	91.5	93
Ni	102.4	1.93	1.995	1.995	1.98	92.5	92.5	95.5
Zn	109.5	1.96		1.995			95	

Note. 2θ: O–M–O angle along the S_4 axis; a_i ($i = y, x, z$): Cr–O spacings; for orientation see Fig. 11. Data derived from the positional parameters in (*1*) ($M = Cu^{2+}$, 298 K) and (*2*) ($M = Ni^{2+}$, 77 K).

O–Cr–O bridges. In the cubic lattice the oxygen coordination is described by three Cr^{3+} ions with identical spacings and CrOCr angles $\alpha \approx 90°$ ($ZnCr_2O_4$ for example; Table I) and one M^{2+} ion, inducing three M–O–Cr angles of equal magnitude. In the tetragonal unit cell of $CuCr_2O_4$ the coordination geometry of the oxygen ligands has considerably changed, as is shown in Fig. 11 for the extremal case of a tetragonal compression of the CuO_4 tetrahedra with $2\theta = 180°$ (square-planar arrangement).

The σ-bonding in the reverse direction of the Cu–O bond in the cubic phase (projection of the three Cr–O bond lengths a on this direction: $3a \cos^2 54.7_5 = a$—Fig. 10) changes to a situation where only two Cr–O bonds contribute to the σ-bonding along this reverse direction ($\cos^2 45° (a_x + a_y) = \frac{1}{2}(a_x + a_y)$), while the third Cr–O bond is orthogonal to the xy-plane (Fig. 11). The "σ-contrapolarizing" power of the three Cr^{3+} ions on the Cu–O bonds is greater in the cubic phase, because the Cr–O bond length a in $ZnCr_2O_4$ is smaller than $\frac{1}{2}(a_x + a_y)$ (Table I). We propose that it is the corresponding strengthening of the Cu–O bond—going from the cubic to the tetragonal phase—which provides the driving force for the enhanced ground state splitting and local distortion of the CuO_4 tetrahedra. Two approaches demonstrate that this kind of microscopic model can indeed account for the experimental findings. A similar consideration for octahedral Cu^{2+} in perovskite-type model compounds gives even more convincing evidence for the validity of such a concept (*21*).

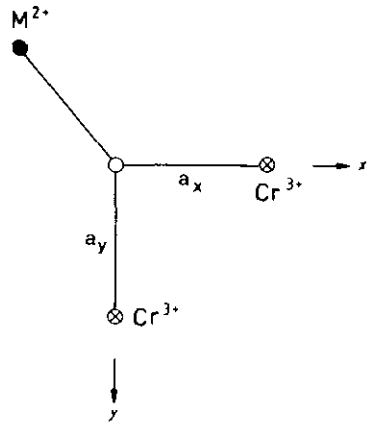

FIG. 11. The oxygen coordination in a tetragonal spinel for the extremal case of square-planar CuO_4 polyhedra (the shortest-distance Cr^{3+} is positioned on the z-axis perpendicular to the figure plane).

In the spinel lattice every CuO_4 tetrahedron is elastically and electronically coupled to four other tetrahedra via eight CrO_6 octahedra, as may be deduced from the cluster in Fig. 10 (left) by geometric extension. For the mentioned cluster we hence have the following expression for the elastic and electronic energy, if it undergoes local and cooperative vibronic coupling:

$$\begin{aligned} E = {} & \tfrac{1}{2} K_e(Q_\theta^2 + q_\theta^2) \\ & + \tfrac{1}{2} K(Q^2 + Q'^2 + Q''^2 + Q'''^2) \\ & - |V_e|(Q_\theta + q_\theta) \\ & - v(Q_\theta + q_\theta)(Q + Q' + Q'' + Q'''). \end{aligned} \tag{20}$$

Here Q_θ, q_θ and Q, Q', Q'', Q''' refer to the

involved CuO_4 and CrO_6 polyhedra, respectively. v is the second order coupling constant for the interaction in the ($OCuO_3Cr_6O_3$ CuO) cluster. Q accounts for the Cr–O bond length changes induced by the cooperative unit cell distortion and can be estimated from the deviations δa from the mean Cr–O spacings,

$$Q = \frac{2}{\sqrt{3}}(|\delta a_x| + |\delta a_y| + |\delta a_z|), \quad (21)$$

where x, y, z stand for the intermediate, long, and short Cr–O bond lengths (Figs. 10, 11; Table I) and $Q^\circ = 0.093$ Å and ≈ 0.023 Å, for $CuCr_2O_4$ and $NiCr_2O_4$, respectively. Minimizing Eq. (20) with respect to Q and $Q\theta$ yields

$$v = KQ^\circ/(Q_\theta + q_\theta) \quad (22a)$$

$$Q_\theta^\circ = (V_e + 4vQ^\circ)/K_e. \quad (22b)$$

With $\rho = 0.44$ Å, $\varphi = 180°$, and the derived V_e and K_e vibronic constants (Section IV.2) one obtains $v = -7000$ cm^{-1} Å^{-2} and $K \simeq 66{,}000$ cm^{-1} Å^{-2} for $CuCr_2O_4$. The latter value is in excellent agreement with reported vibrational data for the Cr–O bond (*22*). For $NiCr_2O_4$—using the vibronic constants and distortion parameters in (*7*)—the cooperative coupling constant is appreciably smaller with $v \simeq 3150$ cm^{-1}Å^{-2}.

If we interpret the cooperative energy $4vQ^\circ$ in Eq. (22b) as being exclusively caused by electronic effects mediated by the ligands, we obtain the equality

$$S_c = 4vQ^\circ. \quad (23)$$

The calculated cooperative strain constant for $CuCr_2O_4$ is $S_c = -2600$ cm^{-1} Å^{-1}, in excellent agreement with the value deduced from the optical data (Section IV.2: -2700 cm^{-1} Å^{-1}). The S_c value for $NiCr_2O_4$ (≈ 300 cm^{-1} Å^{-1}), however, is much smaller than the estimate in (*7*) (1550 cm^{-1} Å^{-1}).

The influence of the M_2–O overlap on the M_1–O bond in a linear M_1–O–M_2 moiety can be studied using the Angular Overlap Model (AOM) (*23*). If a d_z^2 orbital on M_1 interferes with the p_z-orbital on oxygen, the σ-antibonding effect of this interaction can be approximated by perturbation theory in the AOM as

$$e_\sigma = b_{pd\sigma}^2/W, \quad (24)$$

where $b_{pd\sigma}$ is the transfer integral (energy of d–p overlap), W the $L \rightarrow M$ charge transfer energy, and e_σ the relevant AOM parameter. If a second metal ion M_2 is bonded to the same oxygen orbital in the opposite direction (with the AOM parameter $e'_\sigma = b'^2_{pd\sigma}/W'$), e_σ is reduced by

$$\Delta e_\sigma = -e_\sigma e'_\sigma t \quad (t = (W + W')/WW'). \quad (25)$$

The loss in the M_1–O bond strength will be smaller if the M_2–O interaction is diminished—by a growing M_2–O spacing and hence a lowered e'_σ value, for example ($e'_\sigma - \Delta e'_\sigma$)—by the amount

$$\Delta e_\sigma^c = e_\sigma \Delta e'_\sigma t. \quad (25a)$$

The ground state energies of Cu^{2+} in tetrahedral coordination and in a square-planar geometry, as well as the energy gain going from T_d to D_{4h}, are as follows (π contributions neglected) if different e'_σ parameters for the Cr–O overlap with the oxygen p_x, p_y, and p_z orbitals—due to different spacings (Table I)—and hence differing AOM parameters for Cu^{2+} (e_σ^i; $i = x \approx z$, y) are chosen (Figs. 10, 11):

$$\begin{aligned} E(^2T_2, T_d) &= -\tfrac{4}{3} e_\sigma \\ E(^2B_1, D_{4h}) &= -\tfrac{3}{2}(e_\sigma^x + e_\sigma^y). \end{aligned} \quad (26)$$

The energy difference is

$$\Delta E_t(T_d \rightarrow D_{4h}) = -\tfrac{1}{18}(11e_\sigma^{x,z} + 19e_\sigma^y)$$

if the relation $e_\sigma = \frac{1}{3}(2e_\sigma^{x,z} + e_\sigma^y)$ is taken into account. The comparison with the corresponding energy gain ΔE_c, where the Cr–O spacings are identical in the D_{4h} geometry also, yields

$$\Delta E_t - \Delta E_c = -\tfrac{1}{2}(e_\sigma^y - e_\sigma^{x,z}) = -\tfrac{3}{2}\delta e_\sigma, \quad (27)$$

where the difference between e_σ^y ($\equiv e_\sigma$ +

$2\delta e_\sigma$) and $e_\sigma^{x,z}$ ($\equiv e_\sigma - \delta e_\sigma$) is 3 δe_σ. Hence, in the considered case of extremal tetragonal compression ($T_d \rightarrow D_{4h}$), $\frac{3}{2}\,\delta e_\sigma$ can be directly correlated with the energy contribution Δe_σ^c in Eq. (25a), and also with $|S_c|\rho$, where S_c is of the magnitude $4vQ^\circ$ (Eq. (23)).

Concluding, we may state that the physical origin of the increase of the local distortion with increasing M^{2+} concentration in mixed crystals $Zn_{1-x}MxCr_2O_4$ is most likely an increase of the M–O σ-bond strength. The increase is induced by the anisotropy in the spacings of the three Cr^{3+} ions bonded to each oxygen ligand.

4. The Cooperative Strain in Mixed Crystals $Cu_{1-x}Ni_xCr_2O_4$

The ground state potential surfaces of Cu^{2+} and Ni^{2+} in mixed crystals $Cu_{1-x}Ni_x Cr_2O_4$ with tetragonal and orthorhombic unit cells are determined by the individual vibronic coupling constants V_{Ni}, V_{Cu} and by the strain parameters S_{Cu}^c, S_{Ni}^c, which reflect the unit cell distortions due to the cooperative ordering of the CuO_4 and NiO_4 polyhedra. According to the phase diagrams in Figs. 1, 4 and to the $S_c - x$ dependence in Fig. 9 we may assume, that S_{Cu}^c and S_{Ni}^c vanish at $x \approx 0.9$ and $x \approx 0.5$, respectively, and depend linearly on x. We can now define the concentration dependence of the strain parameters:

$$S_{Cu}^c(x) = S_{Cu}(1 - 1.1x) \quad \text{for } 0 \le x \le 0.9$$
$$S_{Ni}^c(x) = S_{Ni}(2x - 1) \quad \text{for } 0.5 \le x \le 1.0. \tag{28}$$

S_{Cu} and S_{Ni} have the magnitudes -2700 and $1700\ cm^{-1}\ Å^{-1}$, respectively. The vibronic energies for Cu^{2+} and Ni^{2+} are now

$$T_2\xi\colon \rho[-(V_{Cu} + S_{Ni}^c)\cos(\varphi - 120) + (\tfrac{1}{2})\,S_{Cu}^c \cos\varphi]$$
$$T_2\eta\colon \rho[-V_{Cu}\cos(\varphi - 240) + (\tfrac{1}{2})S_{Cu}^c\cos\varphi - (\tfrac{1}{2})S_{Ni}^c\cos(\varphi - 120)]$$
$$T_2\zeta\colon \rho[-(V_{Cu} + S_{Cu}^c)\cos\varphi - (\tfrac{1}{2})S_{Ni}^c\cos(\varphi - 120)]$$
$$T_1\alpha\colon \rho'[-(V_{Ni} + S_{Ni}^c)\cos(\varphi' - 120) - (\tfrac{1}{2})S_{Cu}^c\cos\varphi'] \tag{29}$$
$$T_1\beta\colon \rho'[-V_{Ni}\cos(\varphi' - 240) + (\tfrac{1}{2})S_{Ni}^c\cos(\varphi' - 120) - (\tfrac{1}{2})S_{Cu}^c\cos\varphi']$$
$$T_1\gamma\colon \rho'[-(V_{Ni} + S_{Cu}^c)\cos\varphi' + (\tfrac{1}{2})S_{Ni}^c\cos(\varphi' - 120)].$$

Here ρ, φ (ρ', φ') refer to the local distortion of the CuO_4 (NiO_4) tetrahedra. After the addition of the restoring force energies $\frac{1}{2}K_e\rho^2$ (ρ'^2) and minimization of the $T_2\zeta$ and $T_1\alpha$ energies with respect to ρ, φ (ρ', φ') one finds

$$\operatorname{ctg}\varphi_m = \{4(V_{Cu} + S_{Cu}^c) - S_{Ni}^c\}/\sqrt{3}\,S_{Ni}^c \tag{30a}$$
$$\rho_m = \{(V_{Cu} + S_{Cu}^c)\cos\varphi + \tfrac{1}{2}\,S_{Ni}^c\cos(\varphi - 120^\circ)\}/K_e$$
$$\operatorname{ctg}\varphi_m' = -\{V_{Ni} + S_{Ni}^c - S_{Cu}^c\}/\sqrt{3}\,(V_{Ni} + S_{Ni}^c) \tag{30b}$$
$$\rho_m' = \{(V_{Ni} + S_{Ni}^c)\cos(120^\circ - \varphi') + \tfrac{1}{2}\,S_{Cu}^c\cos\varphi'\}/K_e.$$

The values of φ^c, reflecting the symmetry of the lattice distortions ($T = 0$ K), are obtained by minimizing the sum of the ground state energies for Cu^{2+} and Ni^{2+}, weighted by the respective concentration x:

$$E^c = (1 - x)\,E(T_2\zeta) + x\,E(T_1\alpha). \tag{31}$$

The result is

$$\operatorname{ctg}\varphi_m^c = \frac{1}{\sqrt{3}}(2A - 1), \tag{32}$$

with

$$A = \{(1 - x)\,(V_{Cu} + S_{Cu}^c) + \tfrac{1}{2}\,S_{Cu}^c\}/\{x(V_{Ni} + S_{Ni}^c) + \tfrac{1}{2}\,S_{Ni}^c\}.$$

The dependence of φ_m, φ_m', φ_m^c on x is depicted in Fig. 12. The region $0.5 \le x \le$

TABLE II

DISTORTION PARAMETERS ρ_m, φ_m (Cu^{2+}) AND ρ'_m, φ'_m (Ni^{2+}) (Å, °) FOR THE ABSOLUTE MINIMA OF THE GROUND STATE POTENTIAL SURFACE OF $Cu_{1-x}Ni_xCr_2O_4$.

	Cu				Ni			
x	ρ_m	φ_m	E_m	ΔE_m	ρ'_m	φ'_m	E'_m	$\Delta E'_m$
0.2	0.39	180	−1297	697[a]	0.14	151,209	−545	5
0.5	0.32	180	−992	392[a]	0.11	148,212	−487	4
0.6	0.30	178	−931	331[a]	0.16	130	−498	48[a]
0.7	0.29	176	−876	276[a]	0.19	125	−527	77[a]
0.85	0.26	172	−805	206[a]	0.23	121	−595	145[a]
0.90	0.25	171	−786	186[a]	0.24	120	−622	171[a]
0.95	0.26	70,170	−801	201	0.25	120	−661	211[a]
0.99	0.25	70,170	−810	180	0.25	120	−693	243[a]

Note. The ground state stabilization energies E_m (E'_m) and the energy barriers ΔE_m ($\Delta E'_m$) connecting the two lowest minima are also given (cm^{-1}). The parameter values are those of Fig. 6.

[a] In these cases values refer to the lowest energy barrier occurring at $\rho = 0$.

0.9 should approximately reflect the extension of the orthorhombic phase at 0 K (Fig. 5). The calculated φ'_m and φ^c_m angles for $x \leq 0.5$ are misleading in so far as the orthorhombic distortion component for Ni^{2+} is dynamic. This is clearly demonstrated by the very flat potential energy surfaces of Ni^{2+} with energy-barriers below the zero-point vibrational energy (Fig. 6d, Table II). Thus the structurally evident φ'_m and φ^c_m-values are 180°, corresponding to tetragonal unit cells with $c/a < 1$. A similar situation is expected to occur for Cu^{2+} at ≥ 0.9, where the strain from the ferrodistortively ordered compressed NiO_4 tetrahedra again generates a symmetrical double minimum potential, as shown in Fig. 6c. This also implies a dynamic situation for symmetry reasons, though the energy barrier is around 250 $cm^{-1} \cdot \varphi_m$ and φ^c_m would be 120°, in accord with the $c/a > 1$ unit cell deformation. The saddlepoints at ρ_m (Fig. 6) are mostly not the lowest energy barriers, which occur at $\rho = 0$ (Table II). One should also note that the results summarized in Fig. 6 and Table 2 are obtained by including LS-coupling, in contrast to those in Fig. 12.

In the concentration region $0.5 \leq x \leq 0.9$ the Cu^{2+} and Ni^{2+} polyhedra are under the influence of strains originating from the cooperativity of both Ni^{2+} and Cu^{2+}. This reduces the local symmetry of the CuO_4 and the NiO_4 tetrahedra to orthorhombic (T = O K). Analyzing specifically the potential surfaces at $x = 0.70$ and 0.85, one can argue that there is a strong delocalization for the CuO_4 as well as for the NiO_4 tetrahedra even within the lowest vibronic levels, because the energy barriers between the two minima are rather low (Figs. 6e–6h; Table II). For $x = 0.7$ a situation arises where the dynamic delocalization of the vibronic states over the two minima of Ni^{2+} implies an effective φ'_m value rather near to 180°. A similar φ_m value is expected for Cu^{2+}, and hence the effective φ^c_m parameter is of the same magnitude. Similarly, in the case of $x = 0.85$, effective φ_m and φ'_m parameters rather close to 120° should result from the partial vibronic averaging. Thus the phase transition is expected to lead to a tetragonal phase with $c/a > 1$ at higher temperatures. This situation corresponds to the X-ray results for $x \approx 0.87$ (Fig. 7). Apparently our calculations do not reproduce the x-values exactly.

The latter considerations indicate that there is apparently an extensive vibronic delocalization present, which makes the geometry of the NiO_4 and CuO_4 polyhedra nearly equal. A more complete vibronic calcula-

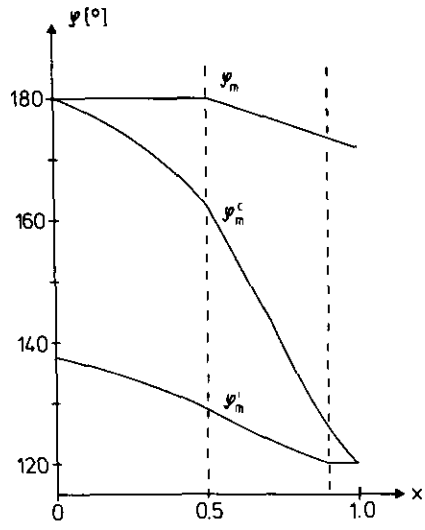

FIG. 12. The dependence of the angular distortion parameters φ on x for mixed crystals $Cu_{1-x}Ni_xCr_2O_4$. φ_m and φ'_m and φ^c_m refer to the CuO_4 and NiO_4 polyhedra and to the averaged distortion of the tetrahedral sites, reflecting the unit cell distortion at 0 K. Parameters as in Fig. 6, but without spin–orbit coupling. Angular values refer to the positions of the lowest minima (see Fig. 6), without taking vibronic delocalization effects into account (see text).

tion, following the one for Cu^{2+} doped Ba_2ZnF_6 (*24*) and taking the vibronic structure of the ground state potential surfaces into account, is in progress. A temperature dependent neutron-diffraction powder study for the mixed crystal with $x = 0.87$ is currently being performed, and the pressure-dependence of the orthorhombic distortion will also be investigated.

Figure 12 depicts the static features of the ground state potential surfaces, taking into account the interplay between local and cooperative Jahn–Teller coupling. If the results are compared with the experiment, electronic and vibrational delocalization effects are apparently very significant. Though the presented results do not reflect the experimental data quantitatively, they reveal that dynamic contributions are of crucial importance. This aspect has not been considered and discussed in literature so far. The φ_m versus x dependence in Fig. 12 is similar to that obtained by Kataoka and Kanamori (*12*), who presented a first analysis of the phase lines of mixed crystals $Cu_{1-x}Ni_xCr_2O_4$. Their model with respect to the tetragonal-to-orthorhombic phase transition is based on a statical disorder of tetragonally compressed CuO_4 and tetragonally elongated NiO_4 tetrahedra of D_{2d} symmetry, however, with $\rho(\rho')$ values independent on x. For the tetragonal region with $c/a < 1$ they assume that random local strains force the S_4 axes of the elongated NiO_4 tetrahedra to orient statistically parallel to the x- and y-directions—a situation which is also favored by entropy. These assumptions are not very realistic, however, because the lattice would have to tolerate local distortions of very different symmetry and extent.

Summarizing, one may state that the vibronic model proposed readily explains that orthorhombic unit cell distortions only occur in a certain concentration range. The NiO_4 tetrahedra adopt the compressed geometry of the CuO_4 polyhedra at $x \leq 0.5$, the deviations from D_{2d} toward an orthorhombic D_2 symmetry being of dynamic nature. Similarly the CuO_4 tetrahedra are tetragonally elongated at $x \geq 0.9$. In the central part of the orthorhombic region around $x \approx 0.85$ the shapes of the potential surfaces for Cu^{2+} and Ni^{2+}, respectively, are such that the dynamics in the zero-point vibronic states seems to create local distortions with $\varphi_m \approx \varphi'_m \approx \varphi^c_m \approx 150°$ (Fig. 7, $x = 0.85$).

V. Concluding Remarks

The purpose of the first part of this contribution was firstly to present a model which explains the increasing electronic ground state stabilization of Cu^{2+} and Ni^{2+} in the tetrahedral sites of the spinel structure with increasing concentration of the Jahn–Teller cations in terms of a microscopic bonding picture on the basis of structural results and data from optical spectra. Second, the geometries of the MO_4 tetrahedra (M: Cu^{2+}, Ni^{2+}) in mixed crystals $Cu_{1-x}Ni_xCr_2O_4$ in the tetragonal and orthorhombic regions

have been analyzed, considering the possibility of dynamic Jahn–Teller contributions to the local distortions.

In a second part, EPR and magnetic data of the considered spinel mixed crystals will be presented.

Acknowledgments

The authors owe thanks to the Deutsche Forschungsgemeinschaft, the Bulgarian Academy of Sciences, and NATO (traveling grant) for financial support. They are also grateful to Professors C. Friebel and W. Massa (Marburg) for helpful discussions.

References

1. E. Prince, *Acta Crystallogr.* **10,** 554 (1957).
2. E. Prince, *J. Appl. Phys.* **32,** 68S (1961).
3. H. Ohnishi and T. Teranishi, *J. Phys. Soc. Jpn.* **16,** 35 (1961).
4. A. Wold, R. J. Arnott, E. Whipple, and J. B. Goodenough, *J. Appl. Phys.* **34,** 1085 (1963).
5. D. Reinen, R. Allmann, G. Baum, B. Jakob, U. Kaschuba, W. Massa, and G. J. Miller, *Z. Anorg. Allg. Chem.* **548,** 7 (1987).
6. D. Reinen and J. Grefer, *Z. Naturforsch. A* **28,** 1185 (1973).
7. D. Reinen, M. Atanasov, G. St. Nikolov, and F. Steffens, *Inorg. Chem.* **27,** 1678 (1988).
8. G. I. Finch, A. P. B. Sinha, and K. P. Sinha, *Proc. R. Soc. London Ser. A* **242,** 28 (1957).
9. P. J. Wojtowicz, *Phys. Rev.* **116,** 32 (1959).
10. R. Englman and B. Halperin, *Phys. Rev. B* **2,** 75 (1970).
11. G. Schröder and H. Thomas, *Z. Phys. B* **25,** 369 (1976).
12. M. Kataoka and J. Kanamori, *J. Phys. Soc. Jpn.* **32,** 113 (1972).
13. J. Kanamori, *J. Appl. Phys.* **31,** 14S (1960).
14. B. Halperin and R. Englman, *Phys. Rev. B* **3,** 1698 (1971).
15. D. Reinen and C. Friebel, *Struct. Bonding (Berlin)* **37,** 1 (1979).
16. F. Hahn and W. Massa, *Z. Naturforch. B* **45,** 1341 (1990); F. Hahn, Thesis, Marburg, 1989.
17. M. Lenglet, J. Lopitaux, and J. Arsene, *J. Solid State Chem.* **50,** 294 (1983).
18. D. Reinen, *Struct. Bonding (Berlin)* **7,** 114 (1969).
19. D. Reinen and M. Atanasov, *Magn. Reson. Rev.* **15,** 167 (1991).
20. F. S. Ham "Electron Paramagnetic Resonance," Plenum, New York (1972).
21. D. Reinen, M. Atanasov, H.-O. Wellern and B. L. Ramakrishna, in preparation.
22. J. R. Ferraro, R. Driver, W. R. Walker, and W. Wozniak, *Inorg. Chem.* **6,** 1586 (1967).
23. H. H. Schmidtke, *Theor. Chim. Acta* **20,** 92 (1971) and cited references.
24. G. Steffen, D. Reinen, H. Stratemeier, M. J. Riley, M. Hitchman, H. E. Mathies, K. Recker, F. Wallrafen, and J. R. Niklas, *Inorg. Chem.* **29,** 2123 (1990).